# RAMAN SCATTERING IN CUPRATE SUPERCONDUCTORS

THOMAS PETER DEVEREAUX
*Department of Physics, George Washington University*
*Washington, D.C. 20052, U.S.A.*

and

ARNO PAUL KAMPF
*Institut für Theoretische Physik, Universität zu Köln*
*Zülpicher Str. 77, 50937 Köln, Germany*

A theory for electronic Raman scattering in the cuprate superconductors is presented with a specific emphasis on the *polarization* dependence of the spectra which can infer the symmetry of the energy gap. Signatures of the effects of disorder on the low frequency and low temperature behavior of the Raman spectra for different symmetry channels provide detailed information about the magnitude and the phase of the energy gap. Properties of the theory for finite T are discussed and compared to recent data concerning the doping dependence of the Raman spectra in cuprate superconductors, and remaining questions are addressed.

*Keywords*: superconductivity, disorder, Raman scattering, oxide superconductors.

## 1. Introduction

Interest in electronic Raman scattering has grown considerably since the first theoretical analysis[1] in 1961 and the subsequent observation of the Raman effect in superconductors seventeen years ago.[2] During the early- to mid- eighties the amount of available data was limited to a few A-15 superconductors while the theory was clarified in many aspects.[3] With the discovery of the high temperature superconductors, this situation dramatically changed as the amount of data grew on these systems. The theory of the Raman effect in superconductors was completed by 1991 for both clean and disordered s-wave superconductors,[4] but this theory could not capture many features shown in experiments on the cuprates. At present, experiments on the Raman effect exist for nearly all "high" temperature superconductors: materials which are electron or hole-doped and materials with different number of $CuO_2$ planes.[5]

Recently attention has turned towards unconventional superconductivity candidates to describe the pairing in the cuprates.[6] Subsequently, due to the strong *symmetry* dependence of the observed spectra, i.e., the characteristic features of light scattering for different incident and scattered polarization orientations, in all high $T_c$ compounds, electronic Raman scattering in unconventional superconduc-

tors has grown to be of considerable interest in light of identifying the symmetry of the energy gap in high temperature superconductors. Indeed, the amount of attention lavished on this area has been remarkable and has provided a large amount of detailed information towards understanding the mechanism of pairing in these materials.

The importance of Raman scattering can be related to its ability to probe excitational dynamics on regions of the Fermi surface rather than being restricted to measuring averages over the Fermi surface. The symmetry dependence of the spectra has augmented an understanding of the magnitude and symmetry of the energy gap, and makes it as effective a probe as photo-emission has proven to be to determine $\Delta(\mathbf{k})$. Moreover Raman scattering is a bulk probe of a material due to the long wavelength of the exciting laser light, does not suffer appreciably from surface effects, and has extremely sharp energy resolution.

Simple considerations of the transformation properties of the light scattering amplitude were used in Ref. 7 to demonstrate how the light polarization orientations selectively probe excitational dynamics of regions of the Fermi surface or the Brillouin zone, and subsequent work has clarified this picture considerably.[8,9,10] In the normal state, the light scattering cross section provides information concerning the scattering rate of electrons in certain $\mathbf{k}$-space regions. $B_{1g}$ scattering geometry $[(x-y)(x+y)$ orientation of incoming (scattered) light polarizations, respectively] probes excitations along the Brillouin zone axes while $B_{2g}$ $[(x)(y)]$ probes the diagonals. Thereby $\mathbf{k}$-dependent scattering processes are measured simply by rotating the polarization orientations of the incoming and scattered photons. In the superconducting state, a $\mathbf{k}$ dependent energy gap can be mapped out. The direct coupling of the Raman vertex to an anisotropic energy gap $\Delta(\mathbf{k})$ leads to a strong polarization dependence of the Raman spectra in the superconducting state. For an energy gap of $d_{x^2-y^2}$ symmetry, which is minimal along the zone diagonals and maximal along the axes, the $B_{2g}$ orientation probes Cooper pairs where the nodes of the gap are located and does not sample regions where the gap is maximal. The reverse is true for the $B_{1g}$ orientation. Thus the $B_{2g}$ spectrum will reflect a smaller energy needed by the incoming light to break a Cooper pair and $B_{1g}$ will have a larger energy scale. Lastly, since $A_{1g}$ involves more of an average around the Brillouin Zone the energy scale can be less than that for $B_{1g}$. Moreover, screening effects for the fully symmetric charge distributions ($A_{1g}$) can drastically reorganize the spectrum for this channel as the long range Coulomb interaction is brought into play.

In most cases, the experimental Raman spectra for optimally hole-doped cuprates can be well modeled using an energy gap of $d_{x^2-y^2}$ symmetry. The relative peak positions, low frequency power-laws and temperature dependence of the nearly elastic contribution for $B_{1g}$ and $B_{2g}$ scattering channels can be naturally explained assuming a $d_{x^2-y^2}$ paired superconducting state. The telling signature here is the presence of an $\omega^3$ frequency dependence of the $B_{1g}$ channel frequencies compared to a linear dependence in other channels. This uniquely identifies the nodal positions of the gap to lie along 45° in the $CuO_2$ plane. However, it is to be noted that a

small linear in frequency contribution is seen in the $B_{1g}$ channel in optimally doped $YBa_2Cu_3O_{7-\delta}$ (Y-123) which may be due to orthorhombic distortions[11] which break the $B_{1g} - A_{1g}$ symmetry distinction and/or may be due to the large Fano distortion of the background due to the 340 $cm^{-1}$ out-of-phase oxygen vibration.[12] For the $A_{1g}$ channel (which can not be purely selected in one particular geometry) the strong peak of the observed spectrum can still be fit by an appropriate choice of the gap and scattering amplitude but the theoretical prediction was found to be extremely sensitive to the number of harmonics used to represent the **k**-dependence and thus to small changes in band structure and/or small dopings. Moreover screening necessarily leads in the calculations to a much smaller signal than seen in experiments. It may be that additional physics is needed to describe the $A_{1g}$ peak shape. However, the linear frequency behavior at small frequencies follows naturally due to a gap with nodes. As in most correlation functions for clean superconductors, only the absolute magnitude of the energy gap and not the phase is measured in Raman scattering. The current agreement of the calculations for clean $d_{x^2-y^2}$ superconductors compared to the data on optimally doped $Bi_2Sr_2CaCu_2O_{8+\delta}$ (Bi-2212) are presented in Fig. 1.

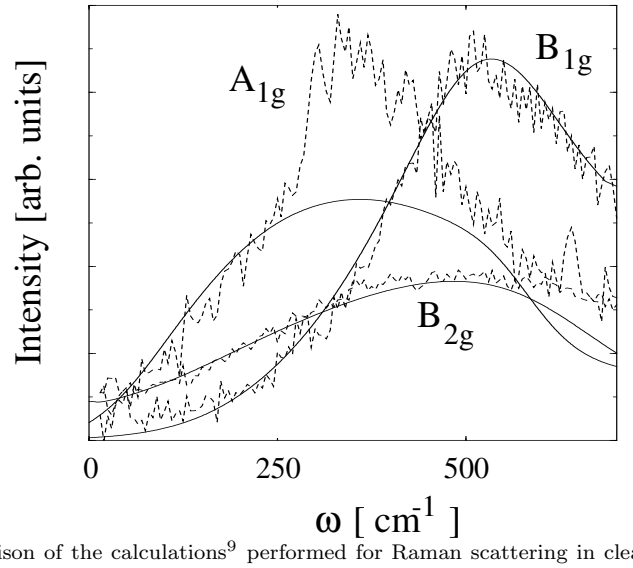


Fig. 1. Comparison of the calculations[9] performed for Raman scattering in clean $d_{x^2-y^2}$ superconductors compared to the data taken on optimally doped Bi-2212 by Staufer et al. in Ref. 5.

However, the theory cannot link a description valid for all temperatures to the normal state. For vanishing momentum transfers of the light, phase space for electronic Raman scattering can only be opened due to scattering via impurities or electron-electron or electron-phonon interactions. In the superconducting state this phase space restriction is lifted since breaking Cooper pairs requires no net momentum transfer.

Building upon the well known results of impurity effects in anisotropic $s$-wave superconductors,[13] Borkowski and Hirschfeld[14] have also shown that while gap anisotropy is unaffected by impurity scattering in $d-$wave superconductors, systematic impurity doping in anisotropic $s-$wave superconductors leads to thermally activated behavior as the gap anisotropy is averaged out and can thus provide an indirect way of determining if the gap has accidental nodal points or if the nodes are enforced by symmetry. Since smearing effects can obscure thermally activated behavior, an observation of a threshold in energy, such as the density of states (DOS), could also be useful. However, it is well known that DOS measurements can be problematic due to surface conditions and small coherence lengths.

Moreover, many open questions are encountered in cuprate superconductors for the Raman spectra away from optimal doping[15]. In overdoped materials a small region (if any) of cubic behavior is seen in the $B_{1g}$ channel before crossing over to a linear low frequency dependence. Strong scattering ($\sim \omega$) is seen down to the lowest frequencies measured in all overdoped materials for all other channels. In underdoped materials, difficulties are encountered to observe features associated with superconductivity in the $B_{1g}$ channel while strong scattering is still seen at low frequencies for all channels and is linear in frequency as well.[16] Additionally the loss of overall scattering intensity of the $B_{1g}$ channel relative to other channels has been taken as evidence for a pseudogap in the normal state.[16] This may be explained as the effect of losing part of the Fermi surface near $(\pi, 0)$ as hole pockets near $(\pi/2, \pi/2)$ are developing. In addition, very distinct features and behaviors are seen in resonant Raman scattering when the incoming laser light is varied, and behavior reminiscent of two-magnon scattering in an antiferromagnetic insulator is seen to persist well into the underdoped region of superconductivity.[17] Therefore, while the existence of spectral weight down to the lowest frequencies implies the existence of a minimum energy gap at most as large as the energy resolution of the experiments, the strong symmetry dependence of the spectra as a function of doping can contain clues to the behavior of excitational dynamics and ultimately a mechanism of pairing for the superconducting state.

While a complete theory now exists for Raman scattering in clean unconventional superconductors, this paper is devoted to augmenting the theory to include the effects of impurity scattering to exploit the fact that the response of a material to deliberate disorder can yield more information concerning the anisotropy of the energy gap but its phase as well. In this paper we will review the theory of Raman scattering in unconventional disordered superconductors with the goal of addressing how the scattering cross section in the superconducting state can provide information on the ground state symmetry as a function of doping. Open questions will be addressed and comparison to the available data will be made.

This paper is outlined as follows: In Section 2 we shall review the essentials of the theory of Raman scattering in metals and confine our attention to the case of only one band crossing the Fermi level. The relation of the symmetry of the Raman vertex and its coupling to an anisotropic energy gap is discussed.

In Section 3 we will present a theory of Raman scattering in disordered unconventional superconductors. Isotropic $s-$wave impurity scattering is included in a gauge invariant way for superconductors with arbitrary gap symmetry at arbitrary temperatures.

Section 4 presents the channel dependent spectra obtained for a $d_{x^2-y^2}$ and an anisotropic $s-$wave superconductor neglecting vertex corrections and are compared and contrasted. The symmetry aspects of the calculations as a function of frequency and temperature are discussed in detail. We also discuss the role of vertex corrections. In particular the existence of disorder generated collective modes are examined.

Lastly, Section 6 compares the results of the calculations to spectra obtained on the cuprates at various dopings. The current agreement and lack of agreement of the data with the theory are discussed, and open questions are presented. A brief account of this work has appeared in Ref. 18.

## 2. General formalism for metals

Electronic Raman scattering measures effective charge fluctuations around the Fermi surface,

$$\tilde{\rho} = \sum_{\mathbf{k},\sigma} \gamma(\mathbf{k}, \mathbf{q} = \mathbf{0}) c^{\dagger}_{\mathbf{k},\sigma} c_{\mathbf{k},\sigma} \tag{1}$$

with a scattering amplitude given by the Raman vertex,

$$\gamma(\mathbf{k}, \mathbf{q} = \mathbf{0}; \omega_I, \omega_S) = \mathbf{e^I} \cdot \mathbf{e^S} + \frac{1}{m} \sum_{\nu} \tag{2}$$
$$\times \left[ \frac{\langle n, \mathbf{k} \mid \mathbf{e^S} \cdot \mathbf{p} \mid \nu, \mathbf{k} \rangle \langle \nu, \mathbf{k} \mid \mathbf{e^I} \cdot \mathbf{p} \mid n, \mathbf{k} \rangle}{\epsilon(\mathbf{k}) - \epsilon_\nu(\mathbf{k}) + \omega_I} + \frac{\langle n, \mathbf{k} \mid \mathbf{e^I} \cdot \mathbf{p} \mid \nu, \mathbf{k} \rangle \langle \nu, \mathbf{k} \mid \mathbf{e^S} \cdot \mathbf{p} \mid n, \mathbf{k} \rangle}{\epsilon(\mathbf{k}) - \epsilon_\nu(\mathbf{k}) - \omega_S} \right],$$

where $\mathbf{e^I}, \mathbf{e^S}(\omega_I, \omega_S)$ are the incident and scattered photon polarization vectors (energies), $\mathbf{p} = -i\hbar\nabla$, and $\epsilon(\mathbf{k})$ and $\epsilon_\nu(\mathbf{k})$ are the Bloch conduction and intermediate state energies, respectively.[3] While in the limit of vanishing light frequencies and for a single band near the Fermi level the Raman scattering amplitude can be related to the curvature of the conduction band, in general this relation does not hold and is of questionable use for the cuprates. A thorough discussion of the Raman vertex is given in the Appendix of Ref. 10. An alternative approach is based on the experimental observation that the spectra near optimal doping in the normal state depends only mildly on the incoming laser light. Then the scattering amplitude can be taken as roughly independent of frequency and symmetry considerations can be given to its $\mathbf{k}-$dependence. This of course misses resonant Raman scattering which will be more relevant for smaller dopings nearer to the antiferromagnetic phase. However, it is a much more complex and unresolved problem of how to bridge non-resonant to resonant scattering.

Therefore we elect to describe the Raman vertex $\gamma$ in terms of an expansion of Fermi surface (FS) or Brillouin zone (BZ) harmonics. The vertices depend on

momentum throughout the BZ as:

$$\begin{aligned} B_{1g}: &\quad \gamma(\mathbf{k}) \sim \cos(k_x a) - \cos(k_y a) + \cdots \\ B_{2g}: &\quad \gamma(\mathbf{k}) \sim \sin(k_x a)\sin(k_y a) + \cdots \\ A_{1g}: &\quad \gamma(\mathbf{k}) \sim \text{constant} + \cos(\mathrm{k_x a}) + \cos(\mathrm{k_y a}) + \cdots , \end{aligned} \tag{3}$$

for a 2-D lattice with lattice constant $a$. Here $\cdots$ represent higher order terms in the BZ expansion. This allows us to correctly classify the anisotropy and transformation properties of the scattering amplitude but leaves open the question of absolute intensities due to the unknown momentum independent prefactors of the expansion. The prefactors can be taken as parameters to fit overall intensities. Apart from $A_{1g}$ (see Ref. 10) the prefactors have only a small effect on the frequency lineshape of the spectra.

The channel-dependent Raman cross section is related to the channel-dependent Raman susceptibility $\chi_{\gamma,\gamma}$ via the fluctuation-dissipation theorem,

$$\begin{aligned} \frac{\partial^2\sigma}{\partial\omega\partial\Omega} &= \frac{\omega_{\mathrm{S}}}{\omega_{\mathrm{I}}}\, r_0^2\, S_{\gamma,\gamma}(\mathbf{q},\omega), \\ S_{\gamma,\gamma}(\mathbf{q},\omega) &= -\frac{1}{\pi}\,[1+n(\omega)]\,\mathrm{Im}\;\chi_{\gamma,\gamma}(\mathbf{q},\omega), \end{aligned} \tag{4}$$

with

$$\chi_{\gamma,\gamma}(i\omega) = \int_0^{1/T} d\tau e^{-i\omega\tau}\langle T_\tau[\tilde{\rho}(\tau)\tilde{\rho}]\rangle, \tag{5}$$

with $T_\tau$ the time-ordering operator and the imaginary part is obtained by analytic continuation, $i\omega \to \omega + i0$. Here $r_0 = e^2/mc^2$ is the Thompson radius and we have set $\hbar = k_B = 1$.

In the absence of impurity scattering, the Raman response function can be written in terms of the $\mathbf{k}-$dependent Tsuneto function

$$\lambda(\mathbf{k}, i\omega) = \frac{\Delta(\mathbf{k})^2}{E(\mathbf{k})^2}\tanh\left[\frac{E(\mathbf{k})}{2T}\right]\left[\frac{1}{2E(\mathbf{k})+i\omega} + \frac{1}{2E(\mathbf{k})-i\omega}\right]. \tag{6}$$

as

$$\chi_{\gamma,\gamma}(i\omega) = \sum_{\mathbf{k}} \gamma^2(\mathbf{k})\lambda(\mathbf{k}, i\omega), \tag{7}$$

with the excitation energy $E^2(\mathbf{k}) = \xi^2(\mathbf{k}) + \Delta^2(\mathbf{k})$, conduction band $\xi(\mathbf{k}) = \epsilon(\mathbf{k}) - \mu$, $\mu$ the chemical potential, and energy gap $\Delta(\mathbf{k})$. We have neglected Coulomb screening (important for fully symmetric charge fluctuations $A_{1g}$) as well as pair interactions responsible for maintaining gauge invariance and collective modes. For details of calculations performed with Eq. (7), the reader is referred to Refs. [7,8,9,10].

From Eqs. (6-7), we see that the Raman vertex couples directly to the energy gap under the momentum summation. Since the $B_{1g}$ channel assigns maximum weight along the BZ axes $(0, \pm 1)$ and $(\pm 1, 0)$, while $B_{2g}$ weights the diagonals $(\pm 1, \pm 1)$, the orientation of the incident and scattering light polarizations thus choose effective

charge fluctuations on the corresponding regions of the FS. Therefore, if for instance a $d_{x^2-y^2}$ energy gap is used, $\Delta(\mathbf{k}) = \Delta_0[\cos(k_x a) - \cos(k_y a)]/2$, the $B_{1g}(B_{2g})$ channel samples regions of the gap maximum (minimum), respectively. The combination of the two symmetries thus gives information about the nodal behavior as well as the maximum value of the energy gap $\Delta_0$.

## 3. Disordered unconventional superconductors

### 3.1. *T-matrix approach*

We now consider the effect of scattering by spinless, noninteracting, isotropic impurities on the Raman susceptibility of unconventional superconductors. We use the self consistent $T-$matrix approach to incorporate repeated scattering events from a single impurity site and dress both the Green's functions as well as the vertex.

The two parameters in this theory are the cotangent of the scattering phase shift, $c = \cot(\delta)$, and the impurity concentration $n_i$ described through the scattering rate $\Gamma = (N/V)n_i/\pi N_F$, where $N/V$ is the electron density and $N_F$ is the density of states per spin at the Fermi level.[19] These enter into the $\hat{T}$-matrix and the self energy in particle-hole (Nambu) space:

$$\hat{\Sigma}(\mathbf{k}, i\omega) = \Gamma \hat{T}(\mathbf{k}, \mathbf{k}, i\omega), \tag{8}$$

The $\hat{T}$ matrix (in terms of the self energy) is depicted in Fig. 2 and satisfies a Bethe-Salpeter equation,

$$\hat{T}(\mathbf{k}, \mathbf{p}, i\omega) = \hat{V}(\mathbf{k}, \mathbf{p}) + \sum_{\mathbf{k}'} \hat{V}(\mathbf{k}, \mathbf{k}')\hat{G}(\mathbf{k}', i\omega)\hat{T}(\mathbf{k}', \mathbf{p}, i\omega), \tag{9}$$

with $\hat{G}$ the Green's function in Nambu space which contains the $\hat{T}$ matrix via Dyson's equation. The matrix $\hat{V}(\mathbf{k}, \mathbf{p})$ is the impurity scattering potential for a single electron, taken to be independent of the electron's spin. Moreover, the potential is taken to be independent of momentum as well to represent $s-$wave scattering only. Therefore the self energy is $\mathbf{k}-$ independent as well.

Expanding the self energy in quarternions, $\hat{\Sigma} = \sum_{i=0}^{3} \hat{\tau}_i \Sigma_i$, where $\hat{\tau}_0$ is the $2 \times 2$ unit matrix and $\hat{\tau}_i (i = 1, 2, 3)$ are the Pauli matrices, the one-particle Green's function can be written as

$$\hat{G}(\mathbf{k}, i\omega) = \frac{i\tilde{\omega}\hat{\tau}_0 + \tilde{\xi}(\mathbf{k})\hat{\tau}_3 + \tilde{\Delta}(\mathbf{k})\hat{\tau}_1}{(i\tilde{\omega})^2 - \tilde{\xi}^2(\mathbf{k}) - \tilde{\Delta}^2(\mathbf{k})}. \tag{10}$$

The tilde indicates the renormalized frequency, gap, and band energy via

$$i\tilde{\omega} = i\omega - \Sigma_0(i\tilde{\omega}), \quad \tilde{\Delta}(\mathbf{k}) = \Delta(\mathbf{k}) + \Sigma_1(i\tilde{\omega}), \quad \tilde{\xi}(\mathbf{k}) = \xi(\mathbf{k}) - \Sigma_3(i\tilde{\omega}). \tag{11}$$

The matrix self energy is given in terms of the integrated Green's function $g_i(i\omega) = \frac{1}{2\pi N_F} \sum_{\mathbf{k}} Tr\{\hat{\tau}_i \hat{G}(\mathbf{k}, i\omega)\}$ as

$$\hat{\Sigma}(i\omega) = \Gamma \frac{g_0(i\omega)\hat{\tau}_0 - g_1(i\omega)\hat{\tau}_1 - c\hat{\tau}_3}{c^2 - g_0^2(i\omega) + g_1^2(i\omega)} = \Sigma_0\hat{\tau}_0 + \Sigma_1\hat{\tau}_1 + \Sigma_3\hat{\tau}_3. \tag{12}$$

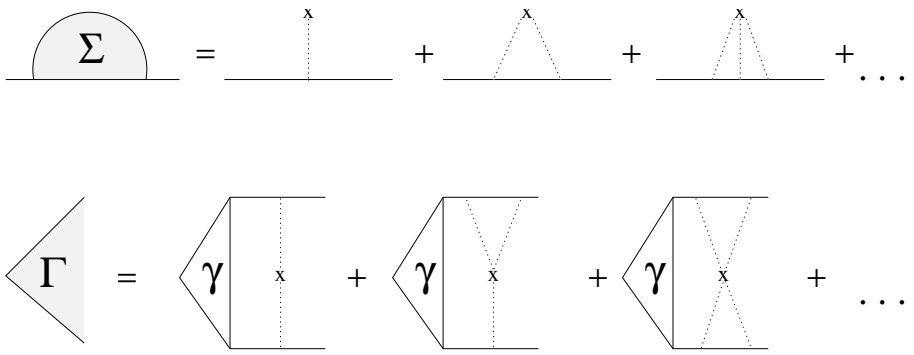


Fig. 2. Diagrams for the T-matrix self energy $\Sigma$ and the renormalized vertex $\Gamma$ as defined in the text.

Here $Tr$ denotes taking the trace. The off-diagonal self energy $\Sigma_1$ is zero only for odd-parity states or states which possess reflection symmetry such as $d_{x^2-y^2}$ or $d_{xy}$. Here we have assumed particle-hole symmetry and further set $g_3(i\omega) = 0$. This allows us to cast the self energy in the simplified form given in Eq. (12). As discussed in Ref. 19, this approximation is valid for either weak (Born, $c >> 0$) or strong (unitary, $c = 0$) scattering provided that impurity vertex corrections play only a minor role. This is shown to be the case in Section 4.3, and therefore we use Eq. (12) for the self energy. For a more detailed discussion of this point, the reader is referred to Ref. 19.

The expression for the Raman response in the limit of vanishing momentum transfer is given by

$$\chi_{\gamma,\gamma}(\mathbf{q} \to 0, i\Omega) = -T \sum_{i\omega} \sum_{\mathbf{k}} Tr\{\gamma(\mathbf{k})\hat{\tau}_3 \hat{G}(\mathbf{k}, i\omega^+)\hat{\tau}_3 \hat{\Gamma}(\mathbf{k}, i\tilde{\omega}^+, i\tilde{\omega}^-)\hat{G}(\mathbf{k}, i\omega^-)\}, \tag{13}$$

where $\omega^{\pm} = \omega \pm \Omega/2$, and $\gamma\hat{\tau}_3, \hat{\Gamma}$ are the bare and impurity renormalized Raman vertices, respectively. The diagrammatic representation for the renormalized vertex is shown in Fig. 2 and can be expressed as the integral equation

$$\hat{\Gamma}(\mathbf{k}, i\tilde{\omega}^+, i\tilde{\omega}^-) = \gamma(\mathbf{k})\hat{\tau}_3 + \sum_{\mathbf{p}} \hat{T}^+ \hat{G}(\mathbf{p}, i\tilde{\omega}^+)\hat{\Gamma}(\mathbf{p}, i\tilde{\omega}^+, i\tilde{\omega}^-)\hat{G}(\mathbf{p}, i\tilde{\omega}^-)\hat{T}^-, \tag{14}$$

with $\hat{T}^{\pm} = \hat{T}(i\tilde{\omega}^{\pm})$.

Eqs. (8-14) form a closed set of equations for the Raman response of unconventional superconductors in the self consistent $\hat{T}$-matrix approximation. We remark that while the impurities are included in a gauge invariant way, the neglect of the pairing interaction in the renormalized vertex does not satisfy gauge invariance and therefore all information regarding the existence of pairing interaction induced collective modes and sum rules is lost. While a gauge invariant treatment is possible

for disordered $s$-wave superconductors[4] a similar treatment has not yet been performed for unconventional superconductors. We note that for clean superconductors, the gauge invariant Raman response has been calculated in Ref. 9 for $d-$ wave superconductors. There it was found that the collective modes which do exist in different Raman channels are damped and lead only to small shifts in the relative peak positions of the Raman spectra in each channel. The low frequency behavior in particular is unaffected. However the Goldstone mode which appears as a consequence of the spontaneously broken $U(1)$ gauge symmetry, provides for both longitudinal and transverse screening of the $A_{1g}$ response in a non-trivial way, as discussed in length in Ref. 9. Therefore we are not in a position to discuss the behavior of the $A_{1g}$ Raman response in the presence of impurities for unconventional superconductors since this would require a gauge invariant treatment.

### 3.2. *Solution of the integral equations*

To solve Equation (14), it is convenient to first remove the $\mathbf{k}-$ dependent term and define $\hat{\Gamma}(\mathbf{k}, i\omega, i\omega') = \hat{\tau}_3\gamma(\mathbf{k}) + \hat{\delta}(i\omega, i\omega')$, and then expand once again in quarternions, $\hat{\delta} = \sum_{i=0}^{3} \hat{\tau}_i\delta_i$. Eq. (14) then turns into a $4 \times 4$ matrix integral equation with no non-zero elements for general $\Delta(\mathbf{k})$. To simplify a solution, we now restrict attention to odd-parity states or states which possess reflection symmetry such as $d_{x^2-y^2}$ or $d_{xy}$. Therefore the energy gap satisfies $\sum_{\mathbf{k}} \Delta(\mathbf{k}) = 0$ and the off-diagonal term of the self energy $\Sigma_1$ can be set to zero. The resulting matrix equation then simplifies to

$$\begin{aligned}
\delta_0 &= \sum_{\mathbf{k}} [I_{00}L^{00}(\mathbf{k})\delta_0 + I_{03}(L^{33}(\mathbf{k})\gamma(\mathbf{k}) + L^{33}(\mathbf{k})\delta_3)] \\
\delta_1 &= \sum_{\mathbf{k}} [I_{11}L^{11}(\mathbf{k})\delta_1 - I_{12}(L^{23}(\mathbf{k})\gamma(\mathbf{k}) + L^{22}(\mathbf{k})\delta_2)] \\
\delta_2 &= \sum_{\mathbf{k}} [I_{11}(L^{23}(\mathbf{k})\gamma(\mathbf{k}) + L^{22}(\mathbf{k})\delta_2) + I_{12}L^{11}(\mathbf{k})\delta_1] \\
\delta_3 &= \sum_{\mathbf{k}} [I_{00}L^{33}(\mathbf{k})(\gamma(\mathbf{k}) + \delta_3) + I_{03}L^{00}(\mathbf{k})\delta_0],
\end{aligned} \tag{15}$$

where we have simplified notation and defined the following:

$$\begin{aligned}
I_{00} &= T_0^+T_0^- + T_3^+T_3^-, \quad I_{11} = T_0^+T_0^- - T_3^+T_3^-, \\
I_{03} &= T_0^+T_3^- + T_3^+T_0^-, \quad I_{12} = -i(T_0^+T_3^- - T_3^+T_0^-),
\end{aligned} \tag{16}$$

and

$$
\begin{aligned}
L^{00}(\mathbf{k}) &= \frac{i\tilde{\omega}^{+}i\tilde{\omega}^{-} + \Delta^2(\mathbf{k}) + \tilde{\xi}^{+}(\mathbf{k})\tilde{\xi}^{-}(\mathbf{k})}{N^{+}(\mathbf{k})N^{-}(\mathbf{k})}, \\
L^{11}(\mathbf{k}) &= \frac{i\tilde{\omega}^{+}i\tilde{\omega}^{-} + \Delta^2(\mathbf{k}) - \tilde{\xi}^{+}(\mathbf{k})\tilde{\xi}^{-}(\mathbf{k})}{N^{+}(\mathbf{k})N^{-}(\mathbf{k})}, \\
L^{22}(\mathbf{k}) &= \frac{i\tilde{\omega}^{+}i\tilde{\omega}^{-} - \Delta^2(\mathbf{k}) - \tilde{\xi}^{+}(\mathbf{k})\tilde{\xi}^{-}(\mathbf{k})}{N^{+}(\mathbf{k})N^{-}(\mathbf{k})}, \\
L^{33}(\mathbf{k}) &= \frac{i\tilde{\omega}^{+}i\tilde{\omega}^{-} - \Delta^2(\mathbf{k}) + \tilde{\xi}^{+}(\mathbf{k})\tilde{\xi}^{-}(\mathbf{k})}{N^{+}(\mathbf{k})N^{-}(\mathbf{k})}, \\
L^{23}(\mathbf{k}) &= \frac{i\Delta(\mathbf{k})[i\tilde{\omega}^{+} - i\tilde{\omega}^{-}]}{N^{+}(\mathbf{k})N^{-}(\mathbf{k})},
\end{aligned}
\tag{17}
$$

with $N^{\pm}(\mathbf{k}) = (i\tilde{\omega}^{\pm})^2 - (\tilde{\xi}^{\pm}(\mathbf{k}))^2 - \Delta^2(\mathbf{k})$.

The matrix equation can then be solved for general vertex $\gamma(\mathbf{k})$. Denoting $\langle A(\mathbf{k})\rangle = \sum_{\mathbf{k}} A(\mathbf{k})$, we obtain the solution to the vertex equation as

$$
\begin{aligned}
\delta_0 &= I_{03}\frac{\langle\gamma(\mathbf{k})L^{33}(\mathbf{k})\rangle + \delta_3\langle L^{33}(\mathbf{k})\rangle}{1 - I_{00}\langle L^{00}(\mathbf{k})\rangle}, \\
\delta_1 &= -I_{12}\frac{\langle\gamma(\mathbf{k})L^{23}(\mathbf{k})\rangle + \delta_2\langle L^{22}(\mathbf{k})\rangle}{1 - I_{11}\langle L^{11}(\mathbf{k})\rangle}, \\
\delta_2 &= \langle\gamma(\mathbf{k})L^{23}(\mathbf{k})\rangle\frac{I_{11} - \frac{I_{12}^2\langle L^{11}(\mathbf{k})\rangle}{1-I_{11}\langle L^{11}(\mathbf{k})\rangle}}{1 - I_{11}\langle L^{22}(\mathbf{k})\rangle + I_{12}^2\frac{\langle L^{11}(\mathbf{k})\rangle\langle L^{22}(\mathbf{k})\rangle}{1-I_{11}\langle L^{11}(\mathbf{k})\rangle}}, \\
\delta_3 &= \langle\gamma(\mathbf{k})L^{33}(\mathbf{k})\rangle\frac{I_{00} + \frac{I_{03}^2\langle L^{00}(\mathbf{k})\rangle}{1-I_{00}\langle L^{00}(\mathbf{k})\rangle}}{1 - I_{00}\langle L^{33}(\mathbf{k})\rangle - I_{03}^2\frac{\langle L^{00}(\mathbf{k})\rangle\langle L^{33}(\mathbf{k})\rangle}{1-I_{00}\langle L^{00}(\mathbf{k})\rangle}}
\end{aligned}
\tag{18}
$$

The conserving approximation for the vertex equation (14) enforces that the impurities have been treated in a gauge invariant way for the the renormalized vertex. However, the full theory is not gauge invariant since the pairing interactions responsible for superconductivity have not been included in the vertex equation.

### 3.3. *Raman susceptibility*

We are now in a position to obtain our final result for the Raman susceptibility. Substituting Eq. (18) into Eq. (13) and performing the trace, the Raman

susceptibility follows as

$$\chi(\mathbf{q}=0,i\Omega)=2T\sum_{i\omega}\Bigg\{\langle\gamma^2(\mathbf{k})L^{33}(\mathbf{k})\rangle$$
$$+\langle\gamma(\mathbf{k})L^{33}(\mathbf{k})\rangle^2\frac{I_{00}+I_{03}^2\frac{\langle L^{00}(\mathbf{k})\rangle}{1-I_{00}\langle L^{00}(\mathbf{k})\rangle}}{1-I_{00}\langle L^{33}(\mathbf{k})\rangle-I_{03}^2\frac{\langle L^{00}(\mathbf{k})\rangle\langle L^{33}(\mathbf{k})\rangle}{1-I_{00}\langle L^{00}(\mathbf{k})\rangle}}$$
$$-\langle\gamma(\mathbf{k})L^{23}(\mathbf{k})\rangle^2\frac{I_{11}+I_{12}^2\frac{\langle L^{11}(\mathbf{k})\rangle}{1-I_{11}\langle L^{11}(\mathbf{k})\rangle}}{1-I_{11}\langle L^{22}(\mathbf{k})\rangle+I_{12}^2\frac{\langle L^{11}(\mathbf{k})\rangle\langle L^{22}(\mathbf{k})\rangle}{1-I_{11}\langle L^{11}(\mathbf{k})\rangle}}\Bigg\}. \tag{19}$$

The first term is the response in the absence of vertex corrections while the next two terms are due to vertex corrections. To obtain the final result for the Raman cross section, one must analytically continue by letting $i\Omega\rightarrow\Omega+i0$ and take the imaginary part of Eq. (19) to be put into Eq. (4).

We now consider the role of symmetry in the vertex corrected response. We focus on $A_{1g}$ scattering first to show its connection to gauge invariance. For isotropic density fluctuations, $\gamma(\mathbf{k})=$ constant, and thus by symmetry the last term in Eq. (19) is zero. Part of the second term is canceled by the first term and we are still left with a finite response at $q=0$ for isotropic density fluctuations. This is due to having a theory which breaks gauge invariance and violates the $f-$sum rule and thus particle number conservation. The density response will be made to vanish when the pair interaction is included in the vertex renormalization and when long-range screening by the Coulomb forces are taken into account. This only affects the results for fully symmetric scattering ($A_{1g}$). We note that for general scattering in the $A_{1g}$ channel, $\gamma(\mathbf{k})$ need not be a constant. However, by symmetry we see that the third term in Eq. (19) vanishes for $A_{1g}$ scattering in $d-$wave superconductors.

Next we consider $B_{1g}$ and $B_{2g}$ scattering channels. Again by symmetry we see that the second term vanishes for both channels. However, the third term contributes for channels with the same symmetry as the energy gap $\Delta(\mathbf{k})$. For a gap with $d_{x^2-y^2}$ pairing, the third term is zero for $B_{2g}$ scattering but contributes for $B_{1g}$. The opposite is true for $d_{xy}$ pairing. Thereby we see that the vertex corrections are very symmetry dependent and can by themselves lead to channel-dependent line-shapes.

In the following section we will discuss the results of the theory in the absence of vertex corrections and at zero temperature to bring out the differences between the results from clean unconventional superconductors. In particular we will investigate how impurity effects can help determine the phase of the energy gap. We defer discussions of the role of vertex corrections to the following section.

## 4. Scattering in the absence of vertex corrections

### 4.1. *T=0 results*

In this section we will calculate the effects of impurities on the Raman spectra for unconventional superconductors by evaluating Eqs. (17-19). To simplify the calculations, in what follows we will work with an approximately cylindrical FS and restrict all momentum averages to the FS. The vertices then depend on azimuthal angle $\phi$ around the FS as

$$\begin{aligned} B_{1g}: &\quad \gamma(\phi) = \sqrt{2}\cos(2\phi) \\ B_{2g}: &\quad \gamma(\phi) = \sqrt{2}\sin(2\phi), \end{aligned} \tag{20}$$

where we also neglect higher order terms. We also neglect band structure details and for simplicity take an infinite band as well. We thus approximate all $\mathbf{k}$ sums as an energy integral times an angular integral around the FS:

$$\sum_{\mathbf{k}} \rightarrow N_F \int d\xi d\Omega_{\mathbf{k}}.$$

The reader is referred to Ref. 9 for a discussion of consequences of the these approximations. For instance we are no longer able to discuss the role of the van Hove singularity. Recent calculations show that the van Hove singularity due to the flat bands located near $(\pi, 0)$ shows up as a peak in the $B_{1g}$ Raman spectrum at an energy $\sim \sqrt{\Delta^2 + \epsilon_{vH}^2}$, where $\epsilon_{vH}$ is the distance in energy of the flat band from the Fermi level near the zone axis (see Ref. 10 and Branch and Carbotte in Ref. 8). However no such van Hove peak, which should be sensitive to band structure and should not be tied to the energy gap, is seen in experiments. Since the van Hove is at higher energies for most systems it is likely that quasiparticle inelastic scattering is sufficiently strong to damp this feature if it exists, or it may be lying at further distances away from the Fermi level and thus have inappreciable residue. In any case we neglect this since impurities are sufficient to suppress the van Hove feature in any case.

In this section we consider specifically a $d_{x^2-y^2}$ paired superconductor, with energy gap $\Delta_d(\phi) = \Delta_0 \cos(2\phi)$ and compare with the results for a hypothetical anisotropic $s-$wave superconductor with $\Delta_s(\phi) = \Delta_0 \mid \cos(2\phi) \mid$. In the absence of impurity scattering, the channel-dependent Raman spectra (as well as the results for other correlation functions) would be indistinguishable. We will consider only the $T = 0$ response and defer consideration of finite temperatures as well as vertex corrections to the next subsection and following section, respectively. Since $\sum_{\mathbf{k}} \Delta(\mathbf{k})$ is not zero for the anisotropic $s$ case, we reinsert the $\Sigma_1$ term into $L^{33}$ ($\Delta$ is replaced by $\tilde{\Delta}$ in Eq. (17)) when evaluating integrals for the vertex uncorrected calculations. This is the only modification needed.

The results of the calculations for unitary scattering $c = 0$ are shown in Figs. 3 and 4 for the $B_{1g}$ and $B_{2g}$ channels for both superconductors. One immediately notices that the impurities smear out the logarithmic divergence of the peak at $2\Delta_0$ for the $B_{1g}$ channel for both superconductors. Moreover, as the scattering rate $\Gamma/\Delta_0$ increases past roughly 0.5, the differences between the peak of the spectra in both channels become less pronounced as the scattering becomes the dominant energy

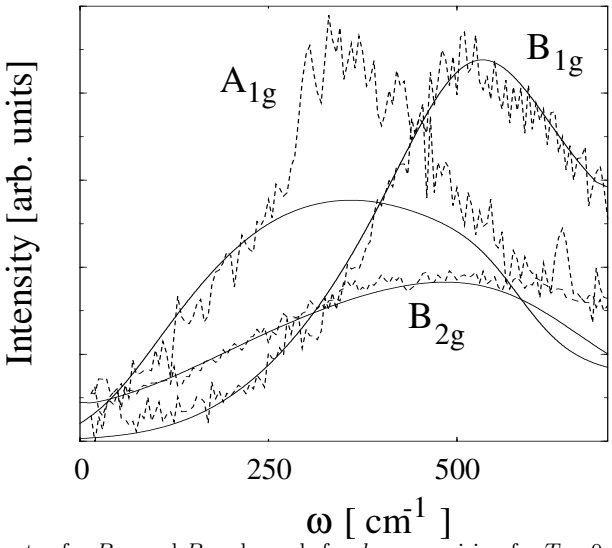


Fig. 3. Raman spectra for $B_{1g}$ and $B_{2g}$ channels for $d_{x^2-y^2}$ pairing for $T = 0$. Values of $\Gamma/\Delta$ are shown for resonant scattering. The inset shows the low frequency behavior on a log-log scale. The $B_{1g}$ spectra show a cross over from $\omega$ to $\omega^3$ at roughly $\omega^* \sim \sqrt{\Gamma\Delta}$. The bounding lines in the $B_{1g}$ insets are guides for $\omega$ (upper) and $\omega^3$ (lower) behavior.

scale in the problem. But as a consequence of the gap renormalization for anisotropic $s$-wave superconductors, $\Sigma_1$ is non zero and the gap becomes averaged out by the disorder and a threshold develops at $\omega_g = 2\Delta_{min}$. For small impurity scattering, this leads to a reduction of the relative peak positions for the $B_{1g}$ and $B_{2g}$ channels compared to $d_{x^2-y^2}$, as shown in Figs. 3 and 4. As the disorder is increased, the peak positions will coalesce and the spectra recover a channel independent, isotropic $s-$wave form, [4]

$$\chi''_{s-wave}(\omega) \sim \Theta(\omega - 2\Delta_{ave})\frac{\Delta_{ave}}{\Gamma} \text{ for } \omega \sim 2\Delta_{\rm ave}$$

with $\Delta_{ave} = 2\Delta_0/\pi$.

However, the main difference for $d_{x^2-y^2}$ and anisotropic $s$-pairing lies in the low frequency behavior, which is very channel dependent, as shown in the insets of Figs. 3 and 4. For clean materials, both superconductors show the characteristic $\omega(\omega^3)$ behavior for the $B_{2g}(B_{1g})$ channels, respectively.

For $d_{x^2-y^2}$ pairing, while impurities do not change the linear in frequency behavior for the $B_{2g}$ channel, below a characteristic frequency $\omega^* \sim \sqrt{\Gamma\Delta}$ the behavior crosses over from $\omega^3$ to $\omega$ for the $B_{1g}$ channel. This is due to a nonzero density of states at the Fermi level, which allows for normal-state-like behavior to be recovered. [20] As in the case of the penetration depth,[21] the scale $\omega^*$ grows with increasing impurity concentrations, and will be shown in the next section to be strongly temperature dependent. However, *the exponent is symmetry dependent* (remains 1 for $B_{2g}$ and $A_{1g}$ channels, while *decreases* from 3 to 1 for the $B_{1g}$ channel). This is in

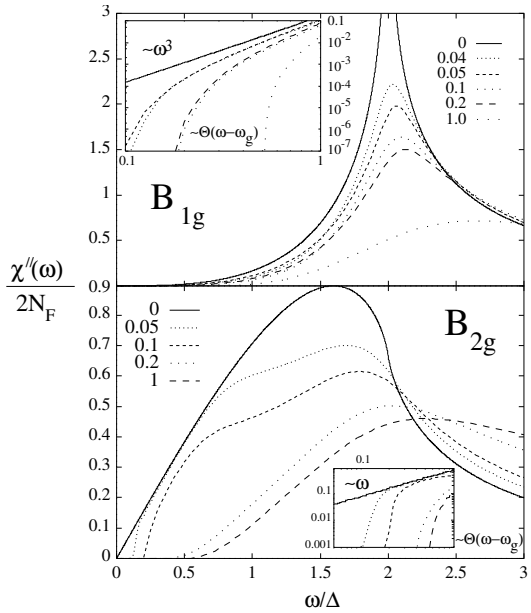


Fig. 4. Raman spectra for $B_{1g}$ and $B_{2g}$ channels for a superconductor with a $\mid d_{x^2-y^2} \mid$ gap symmetry. Inset shows the low frequency behavior which is dominated by a threshold for both channels.

marked contrast to the impurity dependence of the spectra for anisotropic $s$ gap as seen in Fig. 4. The low frequency behavior is dominated by the threshold in this case for *all channels*. Moreover, the impurity dependence of the $B_{1g}$ channel is opposite to what one would expect if the gap was anisotropic $s$-wave. For anisotropic $s$, one sees a transfer of spectral weight out to higher frequencies due to the development of the threshold while for $d_{x^2-y^2}$ the transfer of spectral weight is towards lower frequencies. Thus impurity scattering can provide a clear qualitative way of distinguishing energy gaps of different symmetry.

It can be shown that Born scattering ($c >> 0$) leads to the same effects except for low frequencies. The spectra reorganize at higher frequencies ($\omega \sim 2\Delta_0$) in the same way as for resonant scattering. Also, as has been pointed out[14] there is little difference between Born and unitary scattering for anisotropic $s-$pairing even at low frequencies. However, the low frequency behavior is changed for $d-$pairing. In the Born limit, the low frequency behavior in the $B_{1g}$ channel crosses over from $\omega$ to $\omega^3$ at a much smaller frequency $\omega^*$. Therefore the low frequency behavior of the spectra is similar to the behavior obtained in the absence of impurities except for only very small frequencies in the $B_{1g}$ channel. A substantial linear behavior for $B_{1g}$ can be obtained in the Born limit for large scattering, $\Gamma/\Delta_0 \sim 1 + c^2$, but such a large scattering almost completely smears out the peak feature at $2\Delta_0$.

For small scattering, the threshold generated in anisotropic $s-$ wave superconductors can be obscured via inelastic scattering or experimental resolution. However,

the "effective" exponents for *all* channels would grow as the threshold develops for increased impurity scattering. Since low temperatures and low frequencies can be achieved at high resolution ($\sim 8$ cm$^{-1}$), the smearing can be controlled to allow for a systematic check of the impurity dependence to determine whether the gap has accidental or intrinsic zeroes.

### 4.2. *Finite temperatures*

We now consider the effect of finite temperatures on the calculations. The same physics that is manifest in the symmetry dependent low frequency behavior gives rise to a similar characteristic temperature dependence which can also be used to ascertain the energy gap symmetry.

We first note that for temperatures above T$_c$, the Raman spectrum for channel $L$ is given by a simple Lorentzian:

$$\chi_L''(\Omega, T > T_c) = 2N_F\gamma_L^2 \frac{\Omega\tau}{(\Omega\tau)^2 + 1}, \tag{21}$$

where $\tau = 1/2\Gamma$ is the impurity scattering lifetime.[22] In the presence of vertex corrections $\tau$ becomes channel dependent. This spectrum peaks at frequencies $\Omega = 1/\tau$, rises linearly with frequency and falls off at large frequencies as $1/\Omega$. More complicated forms for $\tau$ can be obtained for $\mathbf{k}-$dependent scattering and when electron-electron interactions are taken into account.[23]

Our results recover this form as $T$ approaches $T_c$. Therefore, any cubic rise of the $B_{1g}$ channel must shrink as temperatures increase and the peak in the spectra must approach the normal state value as well. Both factors lead to a temperature dependence of the crossover frequency $\omega^*$ estimated in the previous subsection.

The temperature dependence of the results for $d_{x^2-y^2}$ superconductors are shown in Figs. 5 and 6. Here we have assumed a weak coupling temperature dependent energy gap for simplicity, whose weak coupling value is $2\Delta_0/T_c = 4.28$. From the Figure it can be seen how the normal state Lorentzian line-shape rises out of the superconducting response as the temperature increases and the energy gap decreases. An additional peak appears at $\Omega = 1/\tau$ in both channels with little weight at low temperatures and increasing in magnitude as the temperature increases. The low frequency behavior is thus dramatically changed so that the spectrum can easily loose any trace of cubic behavior if the impurity scattering and/or the temperature is large enough. Therefore only at very low temperatures can an elastic scattering rate be inferred from the data.

Additional information can be obtained by observing the low frequency behavior as a function of temperature. The ratio of the superconducting response to the normal state response in the static limit $\Omega \to 0$ shows characteristic temperature power-law behavior in the case of clean $d-$wave superconductors as discussed in Refs. 7 and 9. There it was shown that for clean materials the ratio is given by a

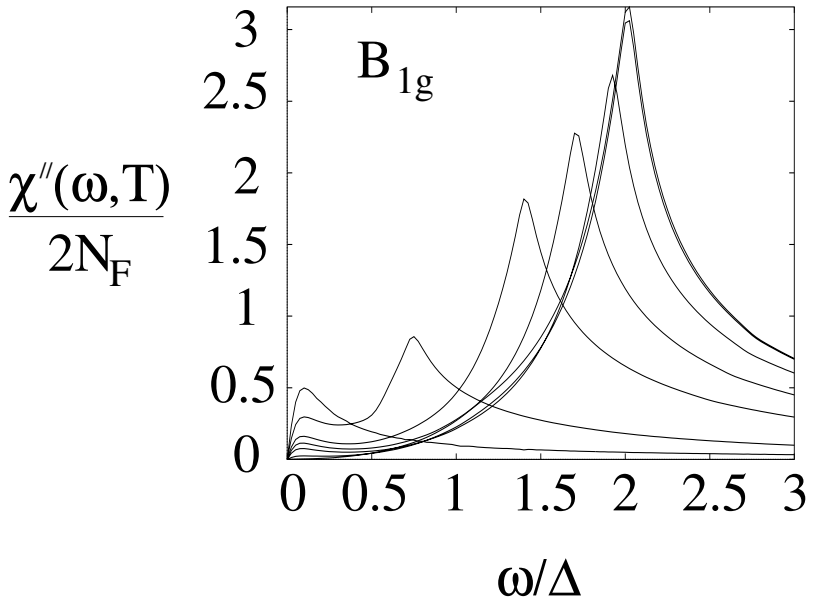


Fig. 5. $B_{1g}$ Raman spectrum evaluated for $\Gamma/\Delta = 0.05$ and for unitary scatterers at successive temperatures $T/T_c = 0.1, 0.5, 0.8, 0.9, 0.99$ and 1, respectively. Here a weak coupling temperature dependence of the energy gap $\Delta/T_c = 2.14$[9] has been assumed for simplicity.

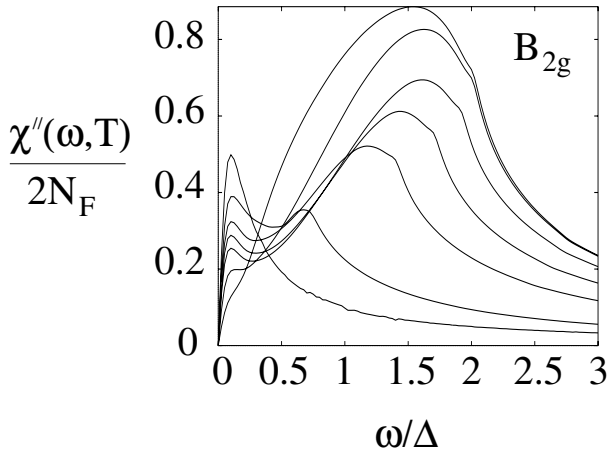


Fig. 6. $B_{2g}$ temperature dependent spectrum using the same parameters as in Fig. 5.

weighted average over the FS of a Fermi function $f$ as

$$\begin{aligned}\frac{\chi''_{s.s.}(\Omega\to 0,T)}{\chi''_{n.s.}(\Omega\to 0,T)} &= \frac{2\langle f(\mid \Delta(\mathbf{k}) \mid) \mid \gamma(\mathbf{k}) \mid^2\rangle}{\langle \mid \gamma(\mathbf{k}) \mid^2\rangle}, \quad \text{clean} \\ &\sim T^3, \qquad T\to 0, \qquad B_{1g}, \\ &\sim T, \qquad T\to 0, \qquad B_{2g}, \end{aligned} \tag{22}$$

where the last two lines gives the same exponents for the low temperature behavior as the exponents for the frequency dependence. It can be seen that the spectra develop a suppression of states at low frequencies faster for the $B_{1g}$ channel than $B_{2g}$, which has been borne out in experiments on clean cuprate samples.[5]

In the presence of disorder this simple expression does not hold. This is due to the fact that the Green's functions do not have an undamped simple pole any longer due to the pair breaking nature of impurities in a $d-$wave superconductor. Moreover, for clean systems above $\mathrm{T}_c$ there is no Raman scattering so this limit is in a sense artificial. The inclusion of impurity scattering verifies the above form if the limit of vanishing scattering is taken as to make the definition sensible. However, for finite scattering the static limit ratio is not given by Eq. (21). For $d_{x^2-y^2}$ pairing, since for all temperatures below $\mathrm{T}_c$ the $B_{2g}$ and $A_{1g}$ channels have a linear dependence on $\Omega$ for small frequencies while even $B_{1g}$ has a small linear dependence as well, this linear dependence mimics the normal state behavior and thus gives a constant term even at $T=0$. Therefore all curves will be shifted upwards at low temperatures.

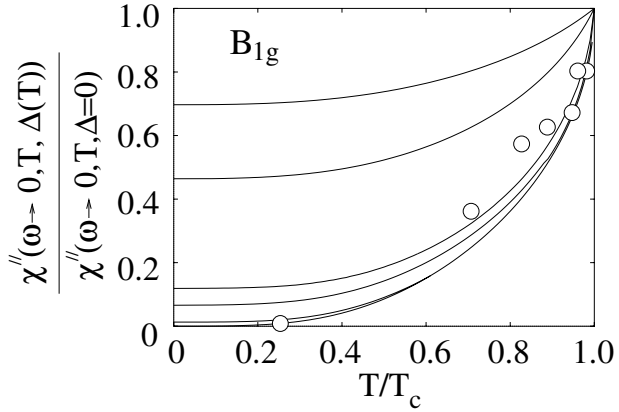


Fig. 7. $B_{1g}$ static ratio as defined in the text as a function of progressively stronger disorder ($\Gamma/\Delta(T=0) = 0, 0.01, 0.05, 0.1, 0.5$ and 1 from bottom to top). The circles are taken from the data of Hackl *et al.* in Ref. 15.

The static ratio for various values of disorder is shown in Figs. 7 and 8 for unitary scattering for a $d_{x^2-y^2}$ paired superconductor. The results are compared to data taken on optimally doped Bi-2212. The number this ratio takes for $T=0$ can

be calculated analytically. If we define $\delta$ as $\delta = \Sigma_0''(\omega \to 0)$ the ratio becomes

$$\frac{\chi''_{s.s.}(\Omega \to 0, T=0)}{\chi''_{n.s.}(\Omega \to 0, T=0)} = \delta^3 \frac{\left\langle \frac{\gamma^2(\mathbf{k})}{(\delta^2+\Delta^2(\mathbf{k}))^{3/2}} \right\rangle}{\langle \gamma^2(\mathbf{k}) \rangle}. \tag{23}$$

This relation shows that in the limit of vanishing scattering, $\delta << \Delta_0$, once again we recover channel dependent exponents. For the $B_{1g}$ channel, Eq. (23) vanishes as $(\delta/\Delta_0)^3$ while for $B_{2g}$ it vanishes linearly in $\delta$.

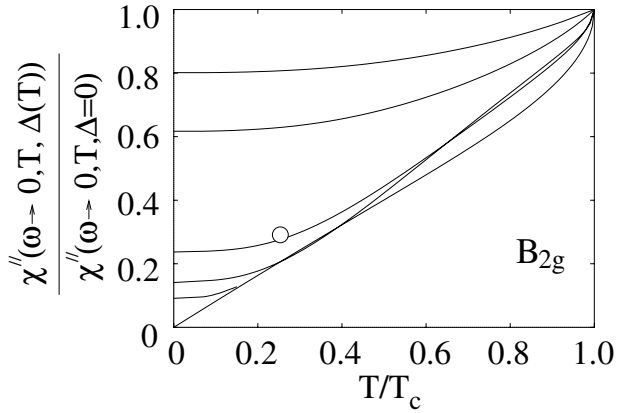


Fig. 8. $B_{2g}$ static ratio as defined in the text as a function of progressively stronger disorder ($\Gamma/\Delta(T=0) = 0, 0.01, 0.05, 0.1, 0.5$ and 1 from bottom to top). The circle is taken from the data of Hackl in Ref. 15.

Finally we determine how large $\delta$ is for both Born and unitary scattering by solving Dyson's equation self consistently.[24] For the case of Born scattering $c >> 1$, then $\delta \sim e^{\Delta_0/\Gamma}$ and is exponentially small. For unitary scattering $c = 0$, $\delta$ is given as a self consistent solution of $\delta \sim e^{\delta^2}$, which is the Omega function $W$ $\delta = 2\sqrt{\Gamma/\Delta_0}/\sqrt{-2W(-\Gamma/\Delta_0)}$. The $W$ function provides logarithmic factors and therefore $\delta \sim \sqrt{\Gamma/\Delta_0}$ in the unitary limit. Therefore for unitary scattering the constant contribution to the static response can be quite large and therefore gives a Raman spectrum which produces normal state behavior with an albeit reduced intensity even at $T = 0$. We note additionally that a constant contribution to the ratio of 20% and 33% has been seen for the $B_{1g}$ and $B_{2g}$ channels, respectively, in Bi-2212 by Yamanaka in Ref. 5.

In closing this section we remark that all calculations have been performed using a weak coupling temperature dependence of the energy gap, which does not provide a good description for the cuprates. However it is trivial to generalize these results to strong coupling energy gaps by using the interpolation formula provided in Appendix B of Ref. 9, which gives the temperature dependence of the gap in analytic form using the specific heat jump and angular averages of the energy gap as input parameters. The above results are only quantitatively changed near $T = T_c$.

Moreover, we have performed all calculations for a 2-D cylinder-like FS and therefore do not capture log corrections that would occur for all low frequency and

temperature behavior of all quantities in 3-D. In the following subsection we will discuss the role of vertex corrections which have been neglected in this subsection as well.

### 4.3. *Vertex corrections*

We return to the expression Eq. (19) for the vertex-corrected Raman response and discuss what changes to the spectra occur when impurity vertex corrections are taken into account. In particular we discuss whether any disorder generated collective modes appear in the spectra and examine any channel dependence which results from the vertex corrections. We remind the reader that we are neglecting vertex corrections from the particle-particle pairing interaction and therefore these results are not truly speaking gauge invariant even though the impurities themselves are treated gauge invariantly.

We limit discussion only to the case for $T = 0$, where the Matsubara sum can be converted into an integral and the analytic continuation to the real frequency axis can be done without having to resort to Padé approximants or other numerical techniques such as maximum entropy.

We first examine whether there exist any collective modes introduced by the disorder for a $d_{x^2-y^2}$ superconductor. We note again that the second term in Eq. (19) is non-zero only for $A_{1g}$ scattering and therefore we only will focus on the third term which is non-zero only in the $B_{1g}$ channel. Therefore there are no impurity vertex corrections for the $B_{2g}$ channel and subsequently no collective modes.

We have searched for frequencies where the real part of the denominator is zero in the second term of Eq. (19) and have not been able to identify the existence of any collective modes. We plot in Fig. 9 the results of the vertex corrected response for the $B_{1g}$ channel and compare them to the results we obtain neglecting vertex corrections. We see that the spectra are essentially unmodified apart from a suppression of spectral weight for frequencies near the gap edge $2\Delta_0$. In particular we do not see a well defined collective mode and the low and high frequency behaviors remain essentially unchanged. Therefore the neglect of vertex corrections does not lead to any substantial changes to the impurity averaged Raman response. This is similar to the results obtained for the pair-interaction-vertex-corrected response obtained in Ref. 9, where it was shown that the vertex corrections lead to essentially no major modifications.

## 5. Comparison to data on cuprate superconductors.

### 5.1. *Optimally and overdoped cuprates.*

In this section we compile our results and compare them to recent data taken on the high $T_c$ cuprates. We remark at the onset that no systematic check of the effects of dopant impurities on the electronic Raman spectra have been undertaken in the metallic state. We do note that doping of Zn [17] and Pr[25] have been inspec-

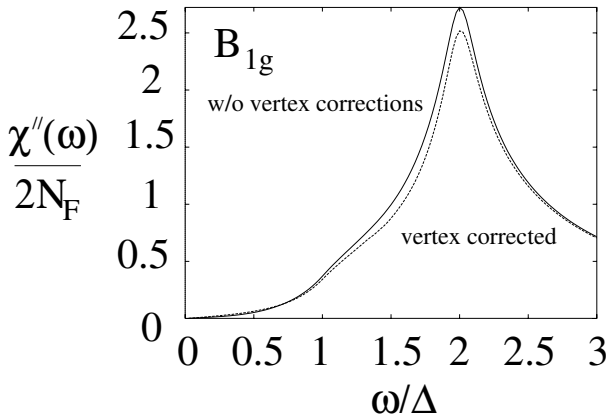


Fig. 9. Comparison of the calculation of the $B_{1g}$ zero temperature spectrum with and without vertex corrections for $\Gamma/\Delta = 0.1$ and unitary scatterers.

ted via Raman scattering on the two-magnon spectra obtained in insulating and underdoped Y-123. There it was seen that the two-magnon feature decreased with the introduction of Zn impurities, while a spectral reorganization of the $A_{1g}$ intensity was observed at roughly a temperature 20 percent higher than $T_c$. Since Zn is believed to seriously distort the local antiferromagnetic order in the $CuO_2$ plane, this finding lends support that antiferromagnetic correlations are strong in these compounds for doping levels where superconductivity is established. The cause of the spectral reorganization for Pr doping is unknown at present.

There is recent evidence which suggests that these materials are *intrinsically* disordered in the overdoped regions of their phase diagram. Measurements of Raman scattering in the normal state of overdoped Bi-2212 by Hackl *et al.* in Ref. 15 have inferred a larger extrapolated zero temperature scattering rate than that obtained for optimal doped samples. Moreover the scattering rate obtained from the $B_{2g}$ channel matched that obtained from D.C. transport.[26] Also, recent muon spin rotation[27] and Hall effect data[28] have suggested that at least for overdoped materials there seems to be intrinsic disorder which is manifest in larger quasiparticle scattering rates.

One possible scenario of how overdoped materials can be considered to be more disordered lies in a crossover argument from 2-D to 3-D behavior. In optimally doped materials, the carriers responsible for superconductivity are confined to the 2-D $CuO_2$ layers. It is known that these materials become more isotropic (c-axis lattice parameter decreases) as they are overdoped.[29] This is manifest in that the c-axis conductivity becomes more and more metallic with overdoping.[30] As the material becomes more 3-D the marginally confined carriers can interact with structural distortions in the charge reservoirs which separate the $CuO_2$ layers. This has been put forth in Ref. 27 as an explanation as to why Ca doping Y-123 (which substitutes Y) leads to a much slower decrease in $T_c$ then Zn doping (which substitutes Cu).

Therefore we will apply the theory as a possible explanation for the channel dependent Raman spectra in overdoped materials. We remark once again that we will treat the energy gap magnitude as a phenomenological parameter to be used to fit the position of the $B_{1g}$ Raman peak and assume $d_{x^2-y^2}$ pairing to be independent of doping[31]. This is not entirely unreasonable since a common feature of the Raman data at *any* polarization is the observance of large intensity at frequencies extending towards vanishing energy transfers, implying the existence of gap nodes. If one were to assume an isotropic $s-$wave energy gap, an explanation would be required in order to produce some smearing mechanism which is as large as 30% of the energy gap to produce the large scattering at low frequencies. Since the resolution of the Raman measurements is less than 10 cm$^{-1}$ and inelastic scattering would be diminished by a factor of $e^{-\Delta_0/T}$, this scenario seems unlikely.

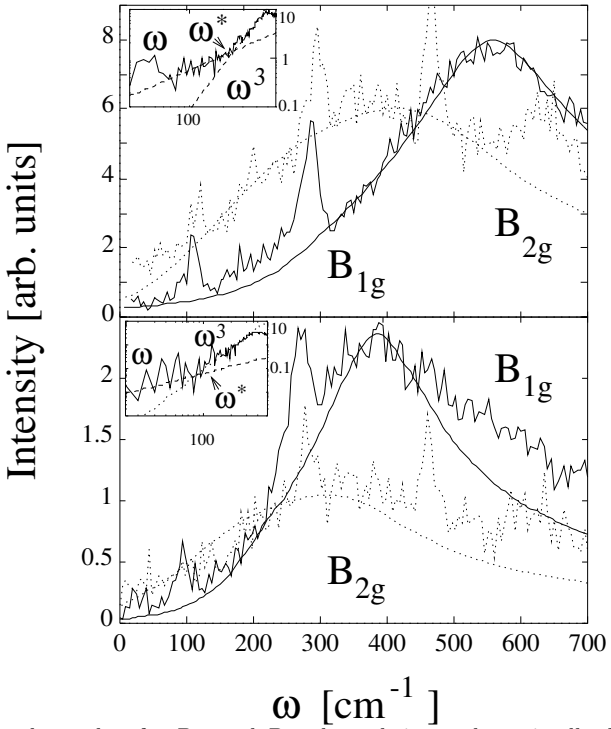


Fig. 10. Fit to the data taken for $B_{1g}$ and $B_{2g}$ channels in nearly optimally doped, as-grown Bi 2212 ($T_c$ = 86 K, top panel) and slightly overdoped $O_2$ annealed Bi 2212 ($T_c$ = 79 K, bottom panel) obtained by Staufer *et al.* in Ref. 5. Here $\Gamma/\Delta_0 = 0.125(0.2)$ and $\Delta_0 = 287(195)\text{cm}^{-1}$ have been used for the top (bottom) panel, respectively. Inset: Log-log plot of the low frequency portion of the $B_{1g}$ response. The crossover frequency $\omega^*/\Delta_0 = 0.38(0.45)$ for the top (bottom) panels, respectively.

We present a fit of theory in Figs. 10 and 11 to the $B_{1g}$ and $B_{2g}$ spectra obtained on nearly optimally doped ($T_c$ = 86K), slightly overdoped ($T_c$ = 79 K), and appreciably overdoped ($T_c$ = 55 K) samples of Bi-2212 taken by Staufer *et al.* in

Ref. 5 and by Hackl *et al.* in Ref. 15. No additional smearing mechanism is invoked. We see that while the peak positions of the data seem to move together as doping is increased the low frequency behavior of the combined data is well accounted for assuming a $d-$wave paired state and an increasing value of the resonant impurity scattering. This is manifest by the growth of the linear contribution of the $B_{1g}$-low-frequency response and the persistence of the $B_{2g}$ linear $\Omega$ behavior. Values of $\Gamma/\Delta_0$ estimated by the crossover frequency which separates linear from cubic behavior in the $B_{1g}$ channel yield $\omega^*/\Delta = 0.38(0.45, 0.58)$ for the optimally (mildly, appreciably over-) doped samples, respectively. Thus spectral weight is being shifted to lower energies as the material becomes more overdoped. This lends supports to the conjecture that these materials are more intrinsically disordered for lower values of $T_c$ on the overdoped side of the phase diagram. However we note that the fit to the appreciably overdoped spectra in Fig. 11, especially the $B_{2g}$ spectrum, is not as good as the fits to the other spectra. The position of the $B_{2g}$ peak cannot be accounted for with our simple theory. Here additional physics seems to be needed. It may be possible that a different number of additional harmonics for the gap function (but still with $d_{x^2-y^2}$ symmetry) may move the peak outward (see Ref. 10 and Branch and Carbotte in Ref. 8). However, without a detailed theory for the pairing mechanism and its doping dependence this remains an open question.

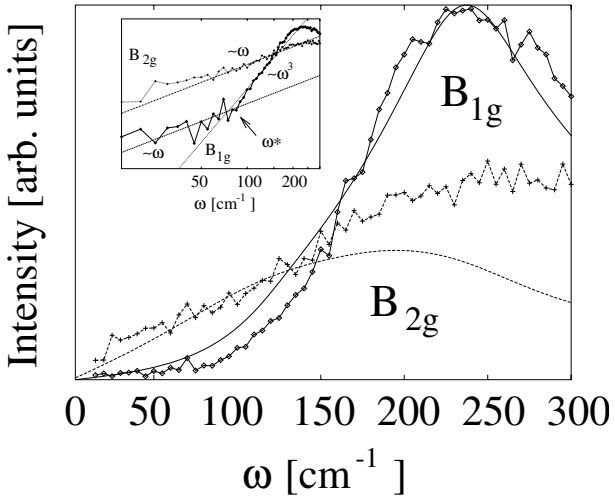


Fig. 11. Fit to the data taken for $B_{1g}$ and $B_{2g}$ channels in appreciably doped Bi 2212 ($T_c = 55$ K) obtained by R. Hackl *et al.* in Ref. 15. Inset: Log-log plot of the low frequency portion of the $B_{1g}$ response. Here $\Gamma/\Delta_0 = 0.22$ and $\Delta_0 = 120\text{cm}^{-1}$ have been used. The crossover frequency $\omega^*/\Delta_0 = 0.58$.

We have neglected quasiparticle inelastic scattering via e.g. spin fluctuations or phonons which will lead to a further smearing of the curves and especially the large peak at $2\Delta_0$ in the $B_{1g}$ channel. However, due to the rapid drop off of the scattering rates at low temperatures and frequencies, the low frequency behavior of the Raman

spectra will not be altered. Inelastic scattering, included phenomenologically in the calculations of Ref. 7 as well as in the calculations of Jiang and Carbotte in Ref. 8, is needed in order to reproduce the normal state behavior for temperatures above $T_c$ as well as the flat background seen at much higher energy shifts even at low temperatures. Thus smaller values of disorder may then be used to fit the data. Moreover, the effect of resonant Raman scattering will be of more importance at higher frequencies and may play a pivotal role for a truly microscopic picture of Raman scattering as a function of doping.

### 5.2. *Conclusions and open problems.*

We close this section by summarizing our results and listing some open questions concerning a more complete picture of Raman scattering in the cuprate materials. We have seen that the theory can provide a satisfactory fit to the low frequency part of the channel dependent Raman response in the cuprate superconductors for optimal doping and for overdoping if we naïvely assume that the main effect of the doping is to introduce intrinsic resonant impurity scattering. This is certainly an open question and an unified picture of what happens even when materials are deliberately disordered via e.g. Zn or Ni doping is still lacking.[32] Moreover, the values of scattering needed to fit the Raman data are indeed quite large to describe the variation of $T_c$ as a function of doping if one applies Abrikosov and Gorkov's theory.[33] As noted, incorporated inelastic scattering could lead to smaller values of disorder needed to fit the data. However, the scattering rates implied by the Raman data match those obtained from D.C. transport, muon spin rotation, and Hall data rather well and do imply increased scattering on the overdoped side of the phase diagram. This still leaves the question of why $T_c$ is not zero unanswered.

One possible scenario is that the scattering due to impurities is highly anisotropic. This evidence comes from the data as well, where both the Raman (see Stadlober *et al.* in Ref. 5 and Hackl *et al.* in Ref. 15) and Hall data[28,36] suggest that scattering is larger along the BZ faces than along the diagonals. If this were true, part of the larger scattering could have the same symmetry as the energy gap and thus not be pair-breaking in the Anderson sense.[34] The theory would have to be changed to incorporate an extended $\mathbf{k}-$dependent impurity potential.[35]

This certainly appears to the case on the underdoped side of the phase diagram which we have not addressed. However, the scattering is most likely inelastic rather than elastic. Issues of anisotropic inelastic quasiparticle scattering near "hot spots" of the FS have been invoked to explain the FS evolution[37] with underdoping as well as transport rates obtained from a Boltzmann approach.[36] It is then clear that including inelastic quasiparticle scattering is a crucial missing point of the theory and is needed to explain the Raman spectra on the underdoped side of the phase diagram. In most Raman experiments, it is difficult to observe any superconductivity related effects in the $B_{1g}$ channel while they still persists for the $B_{2g}$ response.[15] Moreover the relative intensities change as a function of doping in the normal state. For optimally and overdoped material, the Raman intensity in the $B_{1g}$ channel is

always larger than the $B_{2g}$ intensity for any compound measured. However, the $B_{1g}$ intensity has been observed to drop with underdoping and can become smaller than the $B_{2g}$ intensity.[16] This may be related to the loss of the FS around the "hot spots" which are most effectively probed in $B_{1g}$ polarization orientations via the selection rules. Since $B_{2g}$ measures the zone diagonals, the vestige of the FS, or "hole pockets" could still provide for a large electronic Raman signal. It is thus clear that the role of electron-electron interactions and incipient antiferromagnetism will be needed to be incorporated into a theory of Raman scattering for underdoped materials.

Moreover, recent measurements[17] have shown that the Raman spectra for all channels in underdoped materials has a resonance profile that is the same in the normal state as in the superconductor. Therefore one must include resonant Raman scattering processes into the theory even for underdoped materials. This is even more important if one wants to construct a theory for Raman scattering which can be extended to the insulating state and the two-magnon contribution.

Thus in summary, a theory for Raman scattering in unconventional superconductors can be useful to provide insight into the quasiparticle dynamics in high temperature superconductors for various regions of their phase diagram. However many issues are left unresolved and will require further work to build $\mathbf{k}-$space anisotropies and electron correlations into the theory as well as resonant scattering processes. Application of the theory supports recent suggestions that these materials are intrinsically disordered on the overdoped side of the phase diagram, and moreover $d_{x^2-y^2}$ pairing can provide an adequate description of the data.

## Acknowledgments

T.P.D. would like to thank R. Hackl, G. Krug, M. Opel, R. Nemetschek, B. Stadlober, J. C. Irwin, K. Hewitt, and J. Naeni for providing their data prior to publication and for many useful and insightful discussions. T.P.D. would also like to thank J. C. Irwin and his colleagues at Simon Fraser University, where part of this work was completed. We would also like to acknowledge helpful discussions with D. Pines and A. Zawadowski. A.P.K. acknowledges support through a Heisenberg fellowship of the Deutsche Forschungemeinschaft.

## References

1. A. A. Abrikosov and L. A. Fal'kovskii, Zh. Eksp. Teor. Fiz. **40**, 262 (1961) [Sov. Phys. JETP **13**, 179 (1961)].
2. R. Sooryakumar and M. V. Klein, Phys. Rev. Lett. **45**, 660 (1980).
3. A. A. Abrikosov and V. M. Genkin, Zh. Eksp. Teor. Fiz. **65**, 842 (1973) [Sov. Phys. JETP **38**, 417 (1974)]; M. V. Klein and S. B. Dierker, Phys. Rev. B **29**, 4976 (1984); H. Monien and A. Zawadowski, Phys. Rev. B **41**, 8798 (1990).
4. T. P. Devereaux, Phys. Rev. B **45**, 12965 (1992); *ibid.* **47**, 5230 (1993).
5. S. L. Cooper *et al.*, Phys. Rev. B **37**, 5920 (1988); R. Hackl *et al., ibid* **38**, 7133 (1988); S. L. Cooper *et al., ibid.*, 11934 (1988); T. Staufer *et al.*, Phys. Rev. Lett. **68**,

1069 (1992); A. Yamanaka *et al.*, Phys. Rev. B **46**, 516 (1992); R. Nemetschek *et al.*, Phys. Rev. B **47**, 3450 (1993); X. K. Chen *et al.*, Phys. Rev. Lett. **73**, 3290 (1994); *ibid.* Journ. of Supercond. **8**, 495 (1995); A. Hoffmann *et al.*, Physica C **235-240**, 1897 (1994); S. Donovan *et al.*, Journ. of Supercond. **8**, 417 (1995); B. Stadlober *et al.*, J. Phys. Chem. Solids **56**, 1841 (1995); A. Yamanaka *et al.*, in *Spectroscopic Studies of Superconductors*, eds. I. Bozovic and D. van der Marel, Proc. SPIE **2696**, 276 (1996); A. Sacuto *et al.*, LANL cond-mat preprint 9612052.

6. J. Annett, N. Goldenfeld, and A. J. Leggett, to appear in *Physical Properties of High Temperature Superconductors*, Vol. 5, D. M. Ginsberg (ed.), (World Scientific, Singapore, 1996).
7. T. P. Devereaux *et. al.*, Phys. Rev. Lett. **72**, 396 (1994).
8. X. K. Chen *et al.*, Physica C **227**, 113 (1994); **227**, 1089 (1995); M. C. Krantz and M. Cardona, J. Low Temp. Phys. **99**, 205 (1995); D. Branch and J. P. Carbotte, Phys. Rev. B **52**, 603 (1995); **54**, 13288 (1996); C. Jiang and J. P. Carbotte, Solid State Commun. **95**, 643 (1995); Phys. Rev. B **53**, 11868 (1996); W. C. Wu and A. Griffin, Phys. Rev. B **51**, 1190 (1995); **52**, 7742 (1995); O. Narikiyo and K. Miyake, J. Phys. Soc. Jpn. **64**, 3579 (1995); D. Einzel and R. Hackl, J. of Raman Spect. **27**, 307 (1996); M. Cardona *et. al.*, in *Spectroscopic Studies of Superconductors*, eds. I. Bozovic and D. van der Marel, Proc. SPIE **2696**, 182 (1996); T. P. Devereaux, *ibid.*, p. 230.
9. T. P. Devereaux and D. Einzel, Phys. Rev. B **51**, 16336 (1995); *ibid.* **54**, 15547 (1996).
10. T. P. Devereaux, A. Virosztek and A. Zawadowski, Phys. Rev. B **54**, 12523 (1996).
11. T. Strohm and M. Cardona, preprint.
12. T. P. Devereaux, A. Virosztek and A. Zawadowski, Phys. Rev. B **51**, 505 (1995).
13. P. Hohenberg, Zh. Eksp. Teor. Fiz. **45**, 1208 (1963) [Sov. Phys. JETP **18**, 834 (1964)].
14. L. S. Borkowski and P. J. Hirschfeld, Phys. Rev. B **49**, 15404 (1994).
15. F. Slakey *et al.*, Phys. Rev. B **42**, 2643 (1990); X. K. Chen *et al.*, Phys. Rev. B **48**, 10530 (1993); T. Katsufuji *et al.*, Phys. Rev. B **48**, 16131 (1993); R. Hackl *et al.*, J. Low Temp. Phys. **105**, 733 (1996); in *Spectroscopic Studies of Superconductors*, eds. I. Bozovic and D. van der Marel, Proc. SPIE **2696**, 194 (1996); C. A. Kendziora, *ibid.*, p. 223; Phys. Rev. B **52**, 9867 (1995); Phys. Rev. Lett. **77**, 727 (1996); K. Hewitt *et al.*, to appear in Phys. Rev. Lett.
16. J. C. Irwin *et al.* submitted to Phys. Rev. Lett.; R. Hackl *et al.* submitted to Phys. Rev. Lett.
17. G. Blumberg *et al.*, in *Spectroscopic Studies of Superconductors*, I. Bozovic and D. van der Marel (eds.), Proc. SPIE **2696**, 205 (1996); M. Kang *et al.*, Phys. Rev. Lett. **77**, 4434 (1996) and references therein.
18. T. P. Devereaux, Phys. Rev. Lett. **74**, 4313 (1995); Journ. of Supercond. **8**, 421 (1995); J. Phys. Chem. Solids **56**, 1711 (1995).
19. P. J. Hirschfeld *et al.*, Phys. Rev. B **37**, 83 (1988).
20. K. Ueda and T. M. Rice, in *Theory of Heavy Fermions and Valence Fluctuations*, edited by T. Kasuya and T. Saso (Springer, Berlin, 1985); L. P. Gorkov, Pis'ma Zh. Eksp. Teor. Fiz. **40**, 351 (1994) [Sov. Phys. JETP **40**, 1155 (1985)].
21. P. Hirschfeld and N. Goldenfeld, Phys. Rev. B **48**, 4219 (1993); F. Gross *et al.*, Z. Phys. B **64**, 175 (1986).
22. A. Zawadowski and M. Cardona, Phys. Rev. B **42**, 8798 (1990).
23. C. M. Varma *et al.*, Phys. Rev. Lett. **63**, 1068 (1989); B. S. Shastry and B. I. Shraiman, Int. J. Mod. Phys. B **5**, 365 (1991); A. Virosztek and J. Ruvalds, Phys. Rev. Lett. **67**, 1657 (1991); V. N. Kostur, Z. Phys. B **89**, 149 (1992); A. P. Kampf and W. Brenig, Z. Phys. B **89**, 313 (1992).
24. P. A. Lee, Phys. Rev. Lett. **71**, 1887 (1993).
25. M. Rübhausen *et al.*, preprints.

26. C. Kendziora *et al.*, Phys. Rev. B **45**, 13025 (1992); *ibid.* **48**, 3531 (1993).
27. C. Bernhard *et al.*, Phys. Rev. Lett. **77**, 2304 (1996).
28. N. P. Ong in *Physical Properties of High Temperature Superconductors*, ed. by D. M. Ginsberg (World Scientific, Singapore, 1990), Vol. 2; J. P. Rice, J. Giapintzakis, D. M. Ginsberg and J.M. Mochel, Phys. Rev. B **44**, 10158 B. Bucher *et al.*, Phys. Rev. Lett. **70**, 2012 (1993); T. Ito, K. Takenaka, and S. Uchida, Phys. Rev. Lett. **70**, 3995 (1993); A. P. Mackenzie, S. R. Julian, C. T. Lin and D. C. Sinclair, Phys. Rev. B **53**, 5848 (1996).
29. K. Kishio, in *Coherence in Superconductors*, edited by G. Deutscher and A. Revcolevschi (World Scientific, Singapore, 1995).
30. D. N. Basov *et al.*, Phys. Rev. B **50**, 3511 (1994); C. C. Homes *et al.*, Physica C **254**, 265 (1995); preprint.
31. We note that we also are neglecting the important effects of doping and/or disorder on the pairing interaction. This undoubtedly plays a large part of the story concerning $T_c$ suppression, but does not affect the details of the overall lineshape. To proceed further requires a microscopic mechanism for pairing itself.
32. P. J. Hirschfeld, J. Phys. Chem. Solids **56**, 1605 (1995).
33. A. A. Abrikosov and L. P. Gorkov, Pis'ma Zh. Eksp. Teor. Fiz. **40**, 351 (1994) [Sov. Phys. JETP **40**, 1155 (1985)].
34. P. W. Anderson, J. Phys. Chem. Solids **11**, 26 (1959).
35. T. P. Devereaux and A. P. Kampf, unpublished.
36. B. Stojkovic and D. Pines, Phys. Rev. Lett. **76**, 811 (1996); to appear in Phys. Rev. B.
37. A. V. Chubukov, D. K. Morr, and K. A. Shakhnovich, Phil. Mag. B **74**, 563 (1996); D. Pines, preprint.